

RESEARCH ARTICLE

WILEY

A novel design methodology for the compliance of single phase induction motors with recent industrial premium efficiency standards

Ioannis D. Chasiotis | Yannis L. Karnavas 

Laboratory of Electrical Machines,
Department of Electrical and Computer
Engineering, Democritus University of
Thrace, Xanthi, Greece

Correspondence

Yannis L. Karnavas, Laboratory of
Electrical Machines, Department of
Electrical and Computer Engineering,
Democritus University of Thrace, Office
0.21, Building B, Campus, Kimmeria,
Xanthi 671 00, Hellas, Greece.
Email: karnavas@ee.duth.gr

Abstract

The single-phase induction motors (SPIMs) are widely used in several household and industrial applications and thus millions of them are produced every year. Despite the fact that their output power is low, their efficiency enhancement could lead to significant energy savings. The SPIMs are included to the new industrial efficiency standards for commercial motors. Consequently, the minimum efficiency that the SPIMs have to present is that of IE3 (premium-efficiency). The already conducted research efforts have not provided a robust and acceptable—from economical and manufacturing point of view—design procedure toward their efficiency improvement. For this purpose, a novel design methodology is proposed here. It is proven that the required efficiency ratings are achievable with the increment of the motor's axial length, the proper design of the rotor bar slot and the careful selection of the auxiliary to main winding turns ratio along with the value of the used capacitor. Aiming to verify its effectiveness, the presented methodology has been applied to SPIMs with different output power ratings. Moreover, the derived results are compared to the corresponding ones obtained from other design strategies. The motor's nominal performance and its behavior during the start-up phase have been determined through finite element analysis.

KEYWORDS

electrical machine design and manufacturing, high performance motor, premium efficiency standards, single-phase induction motor

1 | INTRODUCTION

The single-phase induction motors (SPIMs) are widely used in numerous low-power household and industrial applications, such as refrigerators, heating-circulating pumps, fans, vacuum cleaners, hair and grain dryers, food mixers, centrifugal, sewing and washing machines, compressors, air conditioners, microwave ovens, conveyor belts, grinders, and so on. Their application field range is quite extensive and they are considered as an attractive, cheap, and reliable solution when the three-phase power supply is not available and thus the three-phase conventional induction motors

This is an open access article under the terms of the Creative Commons Attribution License, which permits use, distribution and reproduction in any medium, provided the original work is properly cited.

© 2020 The Authors. *Engineering Reports* published by John Wiley & Sons, Ltd.

cannot be used. They are manufactured with an output power which ranges from sub-fractional up to few kilowatts. Additionally, they are available in several different types, such as split-phase, capacitor-start/induction-run, shaded pole, capacitor-run and capacitor-start/capacitor-run SPIMs. Among the aforementioned topologies the capacitor-run SPIM seems to gain increased research and industrial interest due to its operational characteristics and its simple structure. It consists of a main and an auxiliary winding which are connected in parallel. At the same time, a capacitor is connected in series with the auxiliary winding during both the motor's starting and running operation. The capacitor does not disconnect the auxiliary winding and consequently no centrifugal switch is required. This feature enhances significantly the motor's reliability and its fault-tolerance. Furthermore, this motor type exhibits¹: (a) low manufacturing cost, (b) silent operation, (c) lower starting current than the other types of SPIMs, and (d) high power factor over a wide speed and load range.

On the other hand, its starting torque and efficiency can be characterized as relatively low. The starting torque is usually equal to 30%-70% of the motor's nominal torque. Concerning the efficiency, it varies from 54.0% up to 74.5% for SPIMs whose horsepower ranges from 0.25 to 1.0 HP according to the data retrieved from the commercial catalogs of several reliable SPIMs manufacturers. The low efficiency has not been considered so far as an important disadvantage due to the fact that these motors are mostly used in low-power applications. However, millions of them are produced every year. Also, research studies have mentioned that the efficiency improvement of the specific motors could lead to significant potential for savings in energy consumption.²

1.1 | Literature review, industrial standards, and motivation of the work

With the present day push for higher efficiency of energy usage, the majority of the developed countries revised the already adopted efficiency standards for electrical motors and proceeded to new mandatory regulations.³ The International Electrotechnical Commission (IEC) has published in March 2014 a new efficiency standard (ie, IEC/EN 60034-30-1). This standard introduces IE4 (super-premium efficiency) efficiency class and also incorporates both single-phase and three-phase squirrel-cage induction motors with 2, 4, 6, and 8 poles. The power range has been expanded to cover motors with output power from 120 W to 1000 kW. The National Electrical Manufacturers Association (NEMA) (ie, the corresponding standards authority in the USA) has published a relevant efficiency standard too. This standard covers a wide scope of general-purpose electric motors and also includes the small SPIMs, whose output power ranges from 0.25 to 3.0 HP. The aforementioned standards are applicable since January 2017⁴ and thus the efficiency ratings of the commercial SPIMs have to comply at least with the specifications of IE3 (premium efficiency) class from now on. The efficiency requirements have been substantially increased. For instance, the minimum efficiency that a 4 poles/1.0 HP SPIM has to present is equal to 82.5% and 85.7% according to IE3 and IE4 efficiency classes respectively.

Therefore, the development of premium efficiency SPIMs is a topic of great interest. In the last few years several research efforts concerning the SPIM's performance improvement have been conducted and various motor's modeling, design, manufacturing, and control aspects have been investigated. In the first place, the researchers proceeded to the development of more accurate models for the calculation of the SPIM's losses. In these models, the impact of eddy currents and also non-linear effects (eg, magnetic saturation on motor's parts) were taken into account.⁵ Moreover, improved equivalent circuits based on the cross-field theory, the forward and backward revolving fields and symmetrical components were proposed in Reference 2 aiming to obtain the best overall motor's performance prediction.

Next, the majority of the research works focused on the determination of the optimal configuration for the squirrel-cage rotor. The rotor bars shape and their geometrical parameters have great effect on the motor's efficiency, power factor, and starting torque and thus this issue was discussed in detail in Reference 6. The final rotor topology of a commercial SPIM has to guarantee two contradictory requirements, that is, the motor's high efficiency during the nominal operation and its satisfactory behavior during the start-up phase. For this reason, numerous rotor slot shapes (eg, trapezoidal, oval, round, rectangular, pent, and so on) and various alternatives (eg, open, semi-closed, closed, shallow or deep rotor bars) have been examined.⁷ Further investigations over the effect of: (a) the rotor bar slot opening and (b) the ratio between the bar's width and height have also been conducted.⁸ Despite the fact that the rotor design procedure has been a process of evolution, it is strongly dependent on the designer's intuition and experience. The incorporation of optimization algorithms and other artificial techniques in the design approach is often necessary.⁹ Another important characteristic that influences significantly the motor's efficiency is the rotor bars number,¹⁰ which is carefully selected along with the poles pairs/stator slots combination. In Reference 11 it is mentioned that greater attention has to be paid

to this decision, as the rotor bars numbers is usually only examined toward the elimination of parasitic phenomena. In this direction, (ie, the minimization of parasitic effects and the motor's performance enhancement) the manufacturers have tested several techniques, such as the inclination of the conventional rotor bars and the construction of skewed rotor slots.¹²

Furthermore, new materials have been tested for the construction of the SPIMs parts. The die-cast copper rotors have replaced the aluminum ones. This can lead to an increment for the efficiency up to 3%.¹³ Several alternative manufacturing techniques have been investigated,¹⁴ but the die-casting process has been established as the most cost-effective solution for the mass production of SPIMs' squirrel-cages.¹⁵ A comprehensive analysis regarding the usage of different rotor bars materials, such as silver and magnesium is provided in References 16,17. The effect of the electrical steels on the SPIM efficiency is reported in Reference 18, while in Reference 19 it is mentioned that the usage of grain-oriented magnetic materials can result to significant energy savings in induction motors. When the utilization of the above materials is combined with the proper formation of the stator structure, the iron losses can be minimized and the temperature alleviation can be enhanced.²⁰ The high quality magnetic materials (ie, electrical steel with high magnetic permeability and low losses density) could be an attractive solution according to Reference 21. However, their cost is prohibitive for low-power applications. Also, it has been proven that when the stator windings are made of aluminum instead of copper, the same efficiency ratings can be achieved, but the windings' mass is smaller and the motor's operation is quite more silent.²²

Another crucial aspect is the capacitor characteristics. The so far research works have focused on the investigations over: (a) the capacitor optimal placement,²³ (b) the proper selection of its value, (c) its impact on the shift angle between the main and the auxiliary windings currents,¹ and (d) the effect of the shift angle on the motor's torque quality.²⁴ It is common knowledge that as the capacitance becomes higher, the starting torque also increases, while the motor's efficiency deteriorates after a specific point. For this reason, the optimal value of the run-capacitor can be determined by incorporating optimization methods, such as the genetic and the particle swarm optimization algorithm.²⁵⁻²⁷ In the above cases, the efficiency of the final optimal SPIM with an output power of 1.0 HP has been found to be equal to 76%. A further efficiency improvement has been achieved in Reference 28, where a SPIM with three in-series connected windings and two capacitors has been proposed. The efficiency of this motor was equal to 80%. However, the motor's cost was also increased, as the capacitors were of high value. A high efficiency of 88% has been recorded in Reference 29 for the case of SPIM with outer rotor topology. The motor's output power was equal to 0.5 HP.

On the basis of the above, it is revealed that a large number of the already examined techniques can contribute to the SPIMs efficiency improvement. However, only few of them are applicable in the mass SPIMs production, as the majority of them introduces increased complexity and high manufacturing cost. This observation reinforces the "strong" opinion of many researchers about the future SPIMs efficiency levels. They claim that their efficiency cannot be enhanced over the ordinary ratings and thus it will be difficult for them to exhibit an efficiency of IE3 according to the latest industrial standards.³⁰ On the other hand, the preliminary results of an authors' recent research effort (ie, Reference 31) indicate that the capacitor-run SPIM's axial effective length increment along with the incorporation of die-cast copper squirrel-cages benefits its efficiency toward IE3. The SPIMs topologies (developed in Reference 31) presented the desirable efficiency, but not adequate starting torque. Also, in that work great emphasis has been given to the impact of rotor bars number, squirrel-cage material and capacitor value on the SPIM performance. No investigation has been conducted regarding the effect of other important design parameters (eg, stator windings turns number, rotor bar design, and so on) which are examined here.

1.2 | Contribution of the work

This article presents an overall integrated and cost-effective design methodology for the development of SPIMs that exhibit: (a) efficiency in accordance with the latest industrial standards and (b) satisfactory starting performance. To make this happen, this work has been split and conducted in two stages.

At the first stage, a sensitivity analysis is performed aiming to highlight the impact of several important design parameters (ie, rotor bar slot cross-sectional area, run-capacitor value, number of main and auxiliary windings turns) on the SPIM's operational characteristics. At the same time, three different design approaches (two modified versions of the classical design methodology and one method introduced by the authors) are examined. These design approaches are described in Section 2. For each one of the derived SPIM topologies, the motor's performance under nominal operation and locked-rotor condition has been determined through finite element analysis (FEA).

At the second stage, the post-processing analysis of the obtained results (given in Sections 3 and 4) contributes to the extraction of useful conclusions, not found elsewhere. Moreover, the limitations and the advantages of the examined design methods are highlighted. Based on these findings, the authors proceeded to the development of a new design methodology, as the major contribution of this work, which limits substantially the search space of the aforementioned design parameters and thus reduces the problem's complexity and computational time. The methodology's effectiveness is validated through its application to SPIMs with different output power ratings and specifications. The description of this methodology and the obtained results are given in Section 5.

Following the provided directions, the SPIMs designers and manufacturers would be able to create an initial capacitor-run SPIM topology (though not optimized) with efficiency at least equal or even higher than the corresponding one defined by the IE3 efficiency class. Consequently, this work: (a) provides strong evidence that the capacitor-run SPIMs can comply with the latest efficiency trends and (b) could be the starting point for further optimization-focused research studies and future commercialization efforts.

2 | DESCRIPTION OF THE EXAMINED DESIGN METHODS

In this section, the important features and steps of the examined design methods are analytically described. The assumptions that the designer has to make by following the classical design procedure are explained and the corresponding authors' proposals and considered modifications are also highlighted. In the first place, the examined design methods have been applied to the case of a capacitor-run SPIM with copper squirrel-cage rotor and an output power equal to 1.0 HP. It is a 4-poles SPIM with 24 stator slots and 30 rotor bars. The geometrical representations of the considered stator and rotor slot topology are depicted in Figure 1. For the rotor bars slot a semi-closed trapezoidal configuration has been selected. It is a simple structure that is frequently selected by many manufacturers. The specifications of the motor under study are summarized in Table A1 in the Appendix. Its operational characteristics and the applied constraints comply with the specifications of commercial SPIMs and the requirements imposed by the latest industrial standards.

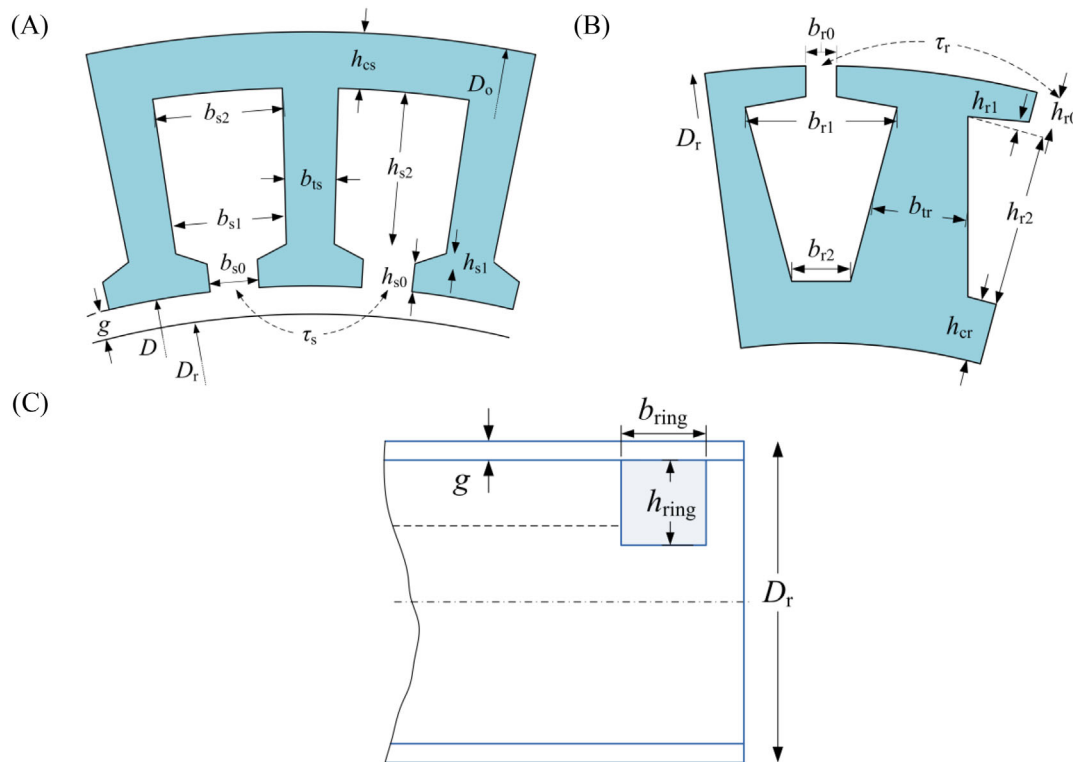


FIGURE 1 Geometrical representation of the SPIM under study: (A) stator topology, (B) rotor slot topology, and (C) axial cross-section of the rotor rings

2.1 | Modified versions of classical design methodology (Method-A and Method-B)

The classical design methodology is a well-known process for both engineers and manufacturers and it is described in detail in Reference 32. It contributes to the development of reliable, but less efficient SPIM topologies, as will be demonstrated later. At first, the designer has to specify the motor's characteristics, such as the supply voltage and frequency, the nominal output power and speed, the desirable efficiency and power factor, the stator/rotor slots combination and the winding type. Next, there is an important design initiation constant to be determined based on past experience. This constant is the machine utilization factor (D_o^2L), which is actually the product of motor's outer stator diameter (D_o) with its axial effective length (L). The calculation of the specific parameter is conducted by means of empirical curves, which represent the variation of D_o^2L as a function of the SPIM horsepower. Typical curves are given in Figure 2 for the case of small induction motors with 2, 4, 6, and 8 poles.

Then, the inner stator diameter (D) to D_o ratio is also empirically taken. This ratio usually ranges between 0.50 and 0.75. Its value is strongly related to the motor's poles number, the electric and magnetic loading. In the case under study, the value of this ratio has been set equal to 0.60. The L/D ratio can be estimated by using Equation (1), where $2p$ is the number of poles and p is the pole pairs. Adopting the formula given there, the L of the obtained SPIM topologies will be smaller than D_o when $2p$ is equal or higher than 4.

$$L/D = \pi \sqrt[3]{p}/(2p) \quad (1)$$

Following the above, we obtain: $D_o^2L = 2376.12 \text{ cm}^3$, $D = 95.25 \text{ mm}$, $D_o = 158.76 \text{ mm}$ and $L = 94.25 \text{ mm}$. The design process continues with the determination of the stator slot geometrical parameters (depicted in Figure 1A) and some of the basic motor's characteristics, such as the airgap length (g) and the rotor's outer diameter (D_r). Further information regarding their analytical calculation is provided in Reference 33.

Proceeding with the rotor topology design, the bars slot dimensions and the end-ring's cross-sectional area (A_{ring}), radial height (h_{ring}) and axial length (b_{ring}) (shown in Figure 1) can be estimated as per the Equations (2)-(7):

$$A_{\text{bar}} = k_{\text{bar}} A_s (Q_s/Q_r) \quad (2)$$

$$2\pi h_{r2}^2 + (2\pi h_{r0} + 2\pi h_{r1} - \pi D_r + Q_r b_{tr} - Q_r b_{r1}) h_{r2} + 2A_r Q_r = 0 \quad (3)$$

$$b_{r2} = (2A_{\text{bar}}/h_{r2}) - b_{r1} \quad (4)$$

$$A_{\text{ring}} = A_{\text{bar}} (2 \sin(\pi p/Q_r))^{-1} \quad (5)$$

$$h_{\text{ring}} = 1.25(h_{r0} + h_{r1} + h_{r2}) \quad (6)$$

$$b_{\text{ring}} = A_{\text{ring}}/h_{\text{ring}} \quad (7)$$

where A_{bar} and A_s are the rotor bar and stator slot area respectively, k_{bar} is the rotor slot area factor, Q_s is the stator slots number, Q_r is the rotor bars number, h_{r0} and h_{r1} are the rotor tooth heights at the opening and at the breaking

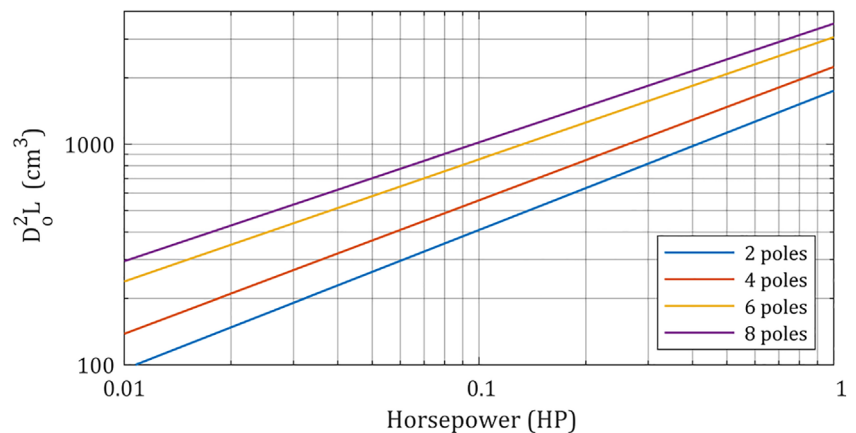


FIGURE 2 Variation of D_o^2L with respect to motor's horsepower³²

respectively, h_{r2} is the net rotor tooth height, b_{tr} is the rotor tooth width, b_{r1} and b_{r2} are the rotor slot widths at the middle and at the top respectively. As it can be seen from Equation (2), the A_{bar} is strongly related to A_s , while simultaneously the slot area factor is involved. Concerning the value that this factor should take, some general directions are provided in Reference 32. It is common practice to choose a value for k_{bar} between 0.35 and 0.60. The designer has to make his own decision and this is the first assumption that the classical design methodology includes. However, the specific decision is quite essential and has great impact on the motor's performance. When k_{bar} takes a high value, the rotor slot area becomes large. This means that the rotor squirrel-cage resistance will be low and consequently the motor will exhibit lower rotor copper losses at nominal operation. When a low value is assigned to k_{bar} , the slot will be shallow and with small cross-sectional area. This results to a higher rotor cage resistance that benefits the motor's starting torque. Consequently, in this point, there is an apparent contradiction.

The next step involves the determination of the main winding turns number (N_m). This quantity is obtained through Equation (8), where E_m is the main winding induced voltage, k_{dis} is the magnetic flux correction factor, B_g is the airgap flux density, k_{wm} is the winding factor of the main winding and f is the power supply frequency.

$$N_m = \frac{2pE_m}{2\sqrt{2}\pi k_{\text{dis}}B_gDLk_{\text{wm}}f} \quad (8)$$

The main winding induced voltage is usually set equal to 0.96 of the supply voltage (U_n). For small SPIMs, B_g and k_{dis} are considered equal to 0.7 and 0.9 respectively. Then, the auxiliary winding turns number (N_a) is estimated by using Equation (9), where a is the turns ratio. The turns ratio value ranges from 1.0 to 2.0. This parameter affects significantly the magneto-motive force and thus the SPIM performance, as mentioned in Reference 34.

$$N_a = aN_m \quad (9)$$

Generally, it is quite difficult for the designer to determine which value of a will result to a motor topology with high efficiency and satisfactory starting torque. In Reference 32 the initial value of the turns ratio is proposed to be set equal to 1.5. Apparently, this is the second important assumption that the classical design methodology includes. Next, the turns ratio value can be properly modified accordingly to the results derived through FEA. However, considering the variation range of this feature, the above process is quite time-consuming.

Finally, the value of the capacitor (C_{run}) can be obtained from Equation (10), where I_n is the motor's nominal current. For the calculation of C_{run} the designer has to assign a value to I_n taking into account the SPIM specifications and the desirable efficiency. However, this is only an initial value for C_{run} , as it does not guarantee the motor's efficiency maximization. The value of C_{run} has to be reassigned if a different turns ratio is adopted. The manufacturers usually use a high value capacitor aiming to enhance the SPIM's starting torque without modifying the rotor bar topology.

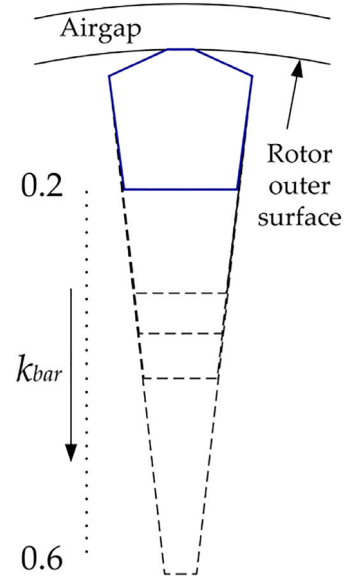
$$C_{\text{run}} = \frac{I_n}{2\pi f U_n (a^2 + 1)} \quad (10)$$

It is easily concluded that many assumptions have to be made when the classical design methodology is adopted. Furthermore, the variation range of the aforementioned parameters is specified by following some general directions. At the same time, two crucial characteristics (ie, the C_{run} and a) are interdependent.

Thus, the authors decided to examine two modified versions of the classical design methodology. For both, the SPIM basic dimensions (ie, L , D and D_o) are determined as previously described.

Method-A: In the first version, the main winding turns number (N_m) is calculated by using Equation (8). The turns ratio value remains constant and equal to 1.5. The run-capacitor (C_{run}) varies from 18 to 30 μF with a step of 1.0. A wider variation range was considered for the k_{bar} compared to the corresponding one proposed in Reference 32. Specifically, the k_{bar} ranges from 0.2 to 0.6 with a step of 0.225. The lower limit for k_{bar} has been selected in such way that the derived rotor bar slots will be easily implemented from manufacturing point of view. The rotor bar topology modification along with the variation of k_{bar} is depicted in Figure 3.

Method-B: In the second version, the N_m is not specified by using Equation (8). This parameter along with a , k_{bar} and C_{run} are set now under investigation. The variation range of k_{bar} and C_{run} is considered equal to the corresponding one adopted in the case of Method-A. Thereinafter, an exhaustive search is conducted for parameters N_m and a . The final selected SPIM topologies present: (a) starting to nominal torque ratio (T_{st}/T_n) at least equal to 0.35 and (b) the highest possible efficiency under these conditions.

FIGURE 3 The rotor bar slot cross-section variation as a function of k_{bar} 

Varying simultaneously the aforementioned design parameters, a large number of different SPIM topologies have been obtained. For each one of them, the motor's performance under nominal operation and locked-rotor condition have been estimated through FEA, as it will be described in Section 2.2.

2.2 | Alternative approach for the selection of SPIM basic dimensions (Method-C)

It was mentioned that the preliminary results of an author's recent work³¹ indicated that the increment of the SPIM's axial effective length benefits the motor's efficiency toward IE3 standards. However, the improved efficiency has to be combined with the satisfaction of many other requirements (eg, adequate starting torque, low starting current, current density, and so on) aiming the SPIMs to comply with the latest international industrial standards. Thus, further investigations have to be performed taking also into account the impact of important design parameters on the motor's operational characteristics. For this purpose, the authors developed another design method (called Method-C from now on). This design method incorporates: (a) all the considerations adopted in Method-B, that is, exhaustive search for k_{bar} , C_{run} , N_m , and a , and (b) an alternative procedure for the calculation of the motor's basic dimensions (ie, D_o , D , and L) compared to the corresponding one described in Section 2.1. The followings steps are involved in the determination of L , D_o , and D :

- Step 1: Select the frame size which coincides with the motor's nominal output power. The dimensions of the frames are defined by the IEC 60072/1 as well as ANSI/NEMA MGI-2010 standards. Reader can find further information about them in Reference 31.
- Step 2: Set the motor's axial effective length (L) equal to the maximum permissible length set by the frame. This will result to motor topologies with L larger than D (the opposite occurs when the classical design methodology is followed).
- Step 3: Determine $D_o^2 L$ by using the corresponding curve from Figure 2 taking into consideration the motor's output power and its poles number.
- Step 4: Calculate D_o for the L obtained in Step 2.
- Step 5: Calculate D by using the D/D_o ratio (equal to 0.6) as mentioned in Section 2.1.

Following the above steps, we obtain: frame size: IEC 90L/NEMA 145T, $D_o = 137.87$ mm, $D = 83.41$ mm, and $L = 125$ mm. The motor's length is now much larger than the corresponding one derived from Method-A and Method-B. This is in accordance with the directions of NEMA for the design and manufacturing of electric motors with longer rotor and stator cores in order to lower the core losses and improve the motor's cooling capability.³⁵ For visualization purposes, the geometrical representations of these two different SPIM designs are depicted in Figure 4.

It must be noted here that for each one of the three previously described design methods a large number of SPIM models have been created and analyzed by using ANSYS® Electromagnetics Suite software (full academic research edition).

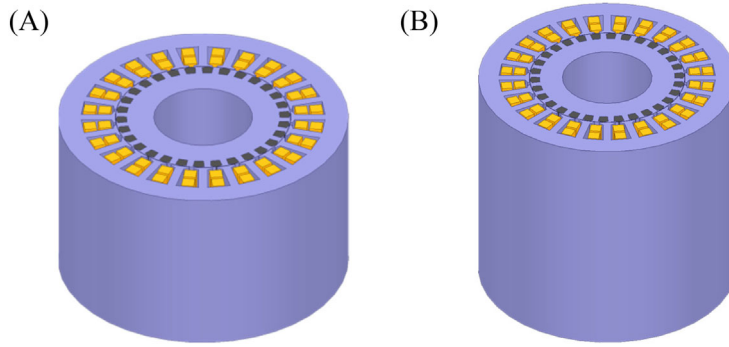


FIGURE 4 Isometric representations (in common scale) of the SPIM models derived from the three examined design approaches, related to D_o and L : (A) classical design methodology modified versions (“Method-A” and “Method-B”) and (B) alternative approach (“Method-C”)

Of course, this procedure is time-consuming, as FEA is included. However, it was necessary aiming to: (a) investigate the impact of these design parameters on several capacitor-run SPIM’s operational characteristics (no research work with similar scope has been found in the up-to-date literature), (b) study the variations of motor’s losses (loss decoupling), (c) find out the limitations and advantages of the three examined design methods, and (d) highlight the mechanisms that contribute to the efficiency enhancement. The motor’s performance under nominal operation and locked-rotor condition has been determined through voltage-driven transient FEA simulations in 2D environment. The calculation of the motor’s stator windings, rotor, capacitor, and iron losses has been conducted by using well-known models which are incorporated in the specific FEA software package. The frictional and windage losses have been determined according to formulas provided in Reference 33 and by taking into account the motor’s specifications (ie, dimensions and angular velocity), the shaft’s (ie, mass and friction coefficient) and bearing’s characteristics (ie, dimensions and bearing load). Typical values (retrieved by the technical reports of reliable shaft and bearings manufacturers) have been adopted for all the involved coefficients.

3 | EFFECT OF C_{run} , K_{bar} , AND A

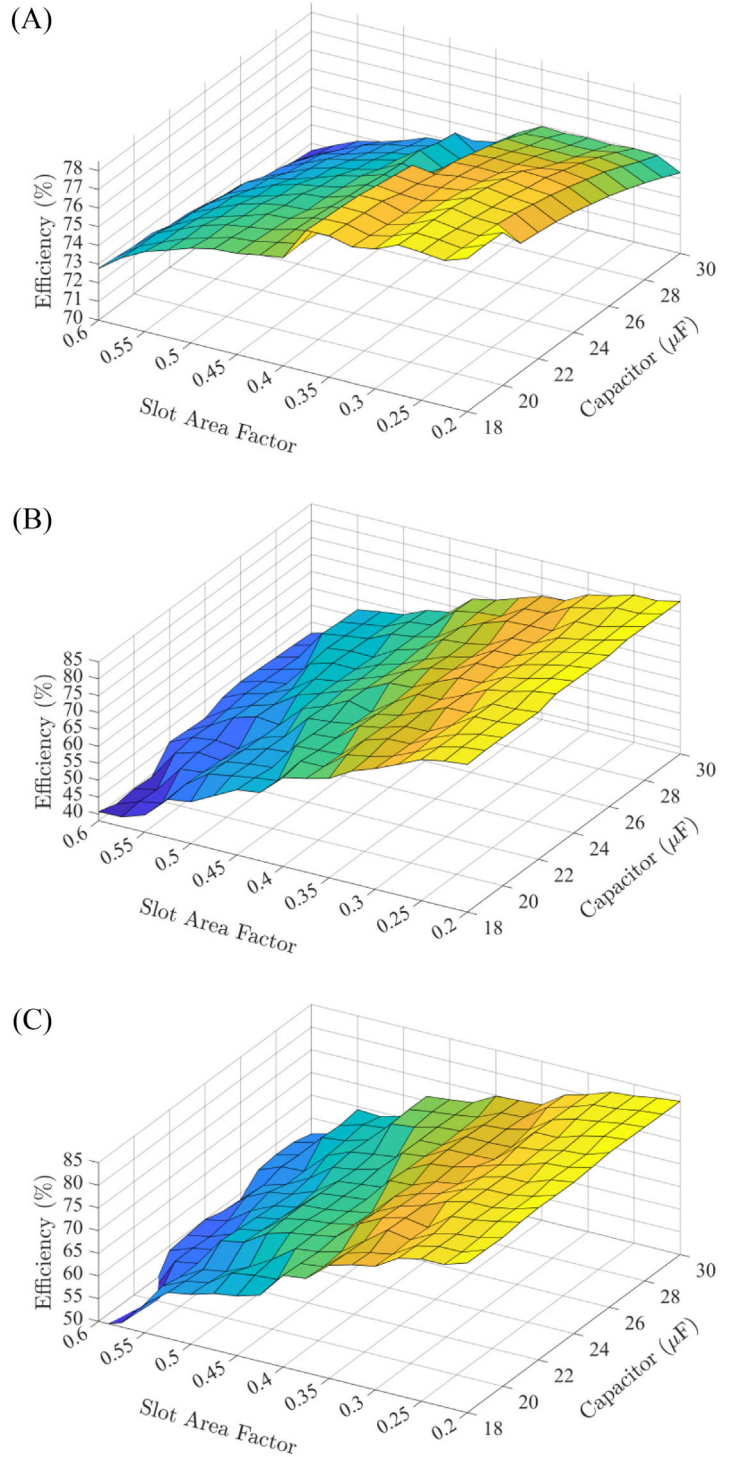
In this section, the effect of C_{run} , k_{bar} , and a on several SPIM’s operational characteristics, such as the efficiency (η), power factor ($\cos \phi$), starting current (I_{st}), and starting to nominal torque ratio (T_{st}/T_n) is presented and analytically discussed. At this point, it must be reminded that the capacitor-run SPIM topologies derived from Method-B and Method-C exhibit T_{st}/T_n ratio higher or at least equal to 0.35. The above has not been considered as requirement when Method-A was followed, where also the turns ratio has been kept constant. By inspecting Figures 5-9 we address and justify here the main findings for each quantity.

3.1 | Efficiency

The motor’s efficiency becomes higher as a smaller rotor bar slot cross-sectional area is used. This can be observed for all the examined design methods (Figure 5). The efficiency acquires its maximum value for $k_{bar} = 0.2$. This can be easily justified by proceeding to loss decoupling. Specifically, when the rotor slot area becomes larger, the stator copper losses (in the main and auxiliary winding) extensively increase due to the higher absorbed motor’s line current. This type of losses is the dominant one and thus determines the tendency of the efficiency. Regarding the core losses significant increment is observed due to the higher recorded magnetic flux density at the rotor’s teeth. The capacitor losses slightly increase, while the frictional and windage losses remain almost the same. Only the rotor bars ohmic losses decrease with the increment of the rotor bar slot area since the rotor cage resistance is lower.

The topologies derived from Method-A present the lowest efficiency. Their minimum and maximum achievable efficiency is equal to 70.6% and 78.2% respectively. The above maximum efficiency value is almost similar to the ordinary SPIMs efficiency ratings of the commercial SPIMs and does not meet the set requirements. Thus, there is a strong evidence that the adoption of Method-A cannot contribute to the development of motors with premium efficiency. Moreover, for a given k_{bar} the efficiency deteriorates as the capacitance becomes higher. The specific quantity decreases up to 4% as the C_{run} varies from 18 μF up to 30 μF due to the higher capacitor and stator copper losses.

FIGURE 5 Variation of SPIM efficiency as a function of C_{run} and k_{bar} for: (A) “Method-A,” (B) “Method-B,” and (C) “Method-C”



The achievement of premium-efficiency is feasible when Method-B and Method-C are adopted. For Method-B, this happens only for $k_{\text{bar}} = 0.2$. For Method-C, motor configurations with efficiency higher than 82.5% can be obtained when the k_{bar} is also equal to 0.225. If the k_{bar} had been set equal to 0.35 (as suggested in Reference 32) the efficiency would be slightly higher than the currently ordinary ratings. All the types of losses, except from the rotor bars ohmic losses, decrease when the value of the capacitor becomes higher. The efficiency enhancement is greater when a rotor bar slot with large cross-sectional area is used. For a low value of k_{bar} the efficiency can be improved up to 2% with a higher capacitance. The SPIM efficiency is maximized for a specific value of C_{run} . Generally, the efficiency gets its maximum value when the C_{run} ranges from 25 μF to 30 μF for all the examined variation range of k_{bar} . For example, for $k_{\text{bar}} = 0.2$ the maximum efficiency is achieved for $C_{\text{run}} = 27 \mu\text{F}$ when the Method-B is adopted. For Method-C the same happens for $C_{\text{run}} = 26 \mu\text{F}$.

3.2 | Power factor

The decrement of k_{bar} with the simultaneous increment of C_{run} benefits substantially the power factor (Figure 6). For given C_{run} and as the rotor bar slot cross-sectional area becomes larger, the specific characteristic presents slight variation for the case of Method-A. The obtained values range from 0.68 to 0.82. These values are considered as low compared to the corresponding ones imposed by the latest industrial trends. Thus, this is another important disadvantage of Method-A. Following Method-B and Method-C the power factor acquires significantly higher values even for a low value of C_{run} . Indicatively, it is mentioned that for Method-C and $k_{\text{bar}} = 0.2$ the power factor varies from 0.95 to 1.0 along with the

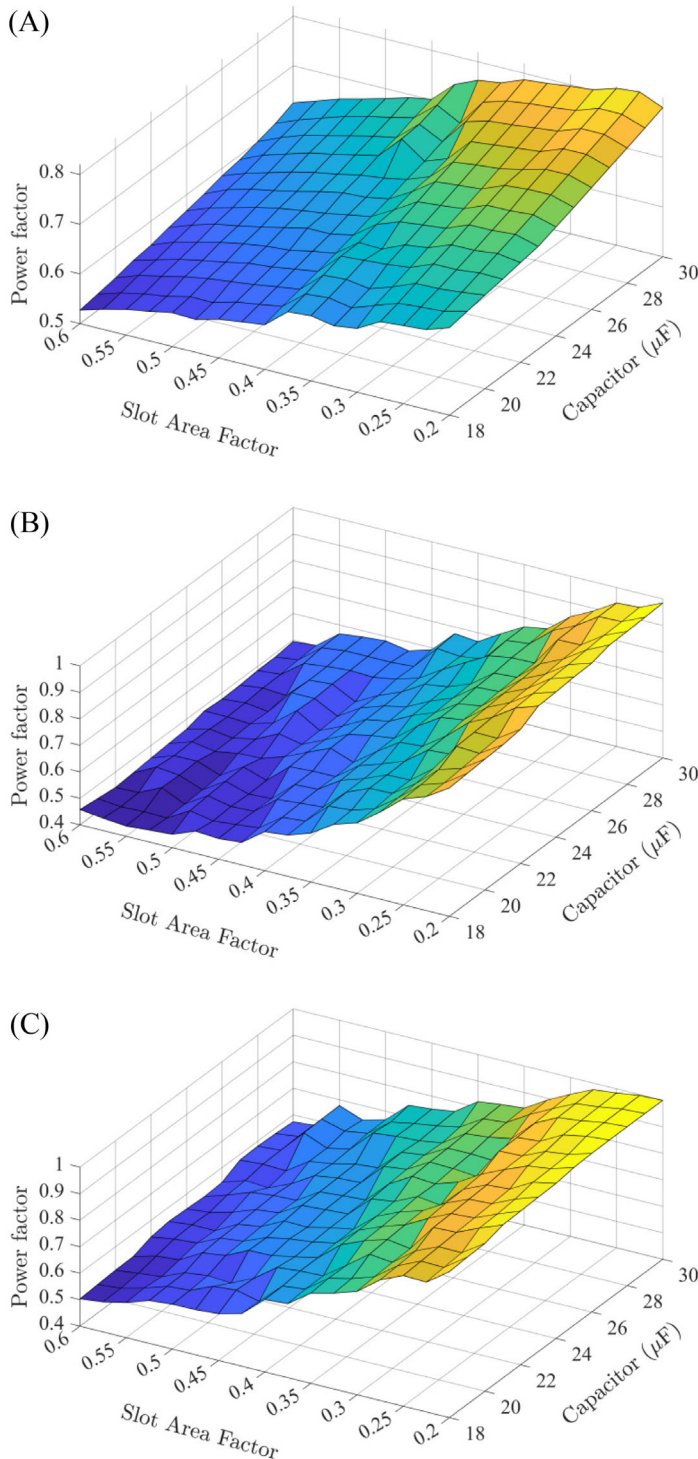


FIGURE 6 Variation of power factor as a function of C_{run} and k_{bar} for: (A) “Method-A,” (B) “Method-B,” and (C) “Method-C”

capacitor value. For the same considerations the value of the power factor ranges from 0.89 to 0.98 when Method-B is adopted.

3.3 | Starting to nominal torque ratio

All the examined models derived from Method-B and Method-C succeeded to fulfill the set requirements for this quantity (Figure 7). This does not happen for the case of Method-A. In this case, the starting torque increases as the rotor bar cross-sectional area becomes smaller and a high value is used for C_{run} . Specifically, when k_{bar} was equal or higher than 0.35 the starting torque was low regardless of the C_{run} value. Consequently, only 49 out of the 221 investigated motor topologies exhibit T_{st}/T_n ratio at least equal to 0.35. In some cases the above ratio acquires values up to 0.64 and thus

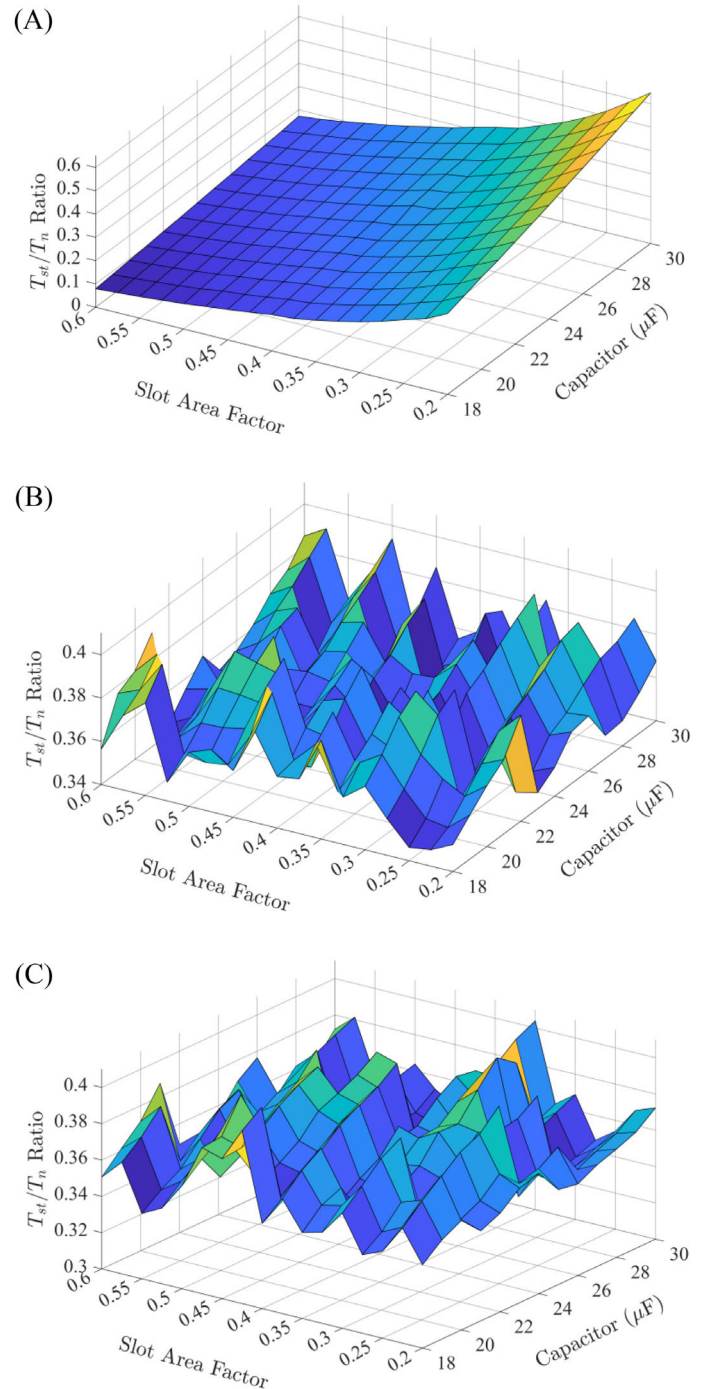


FIGURE 7 Variation of SPIM starting to nominal torque ratio as a function of C_{run} and k_{bar} for (A) “Method-A,” (B) “Method-B,” and (C) “Method-C”

SPIM topologies with high starting torque can be obtained. This could be an attractive characteristic as there are few applications where a great amount of torque is needed during the start-up phase. To make this happen, a high value of C_{run} is required. However, as already mentioned the increment of the capacitor value reduces the motor's efficiency when Method-A is followed. Thus, the high starting torque for the motor is combined with a low efficiency.

3.4 | Starting current

Generally, it can be said that the motor's starting current decreases significantly as the rotor bar slot cross-sectional area becomes smaller and a high value is assigned to C_{run} (Figure 8). A smaller variation is observed for Method-A. The

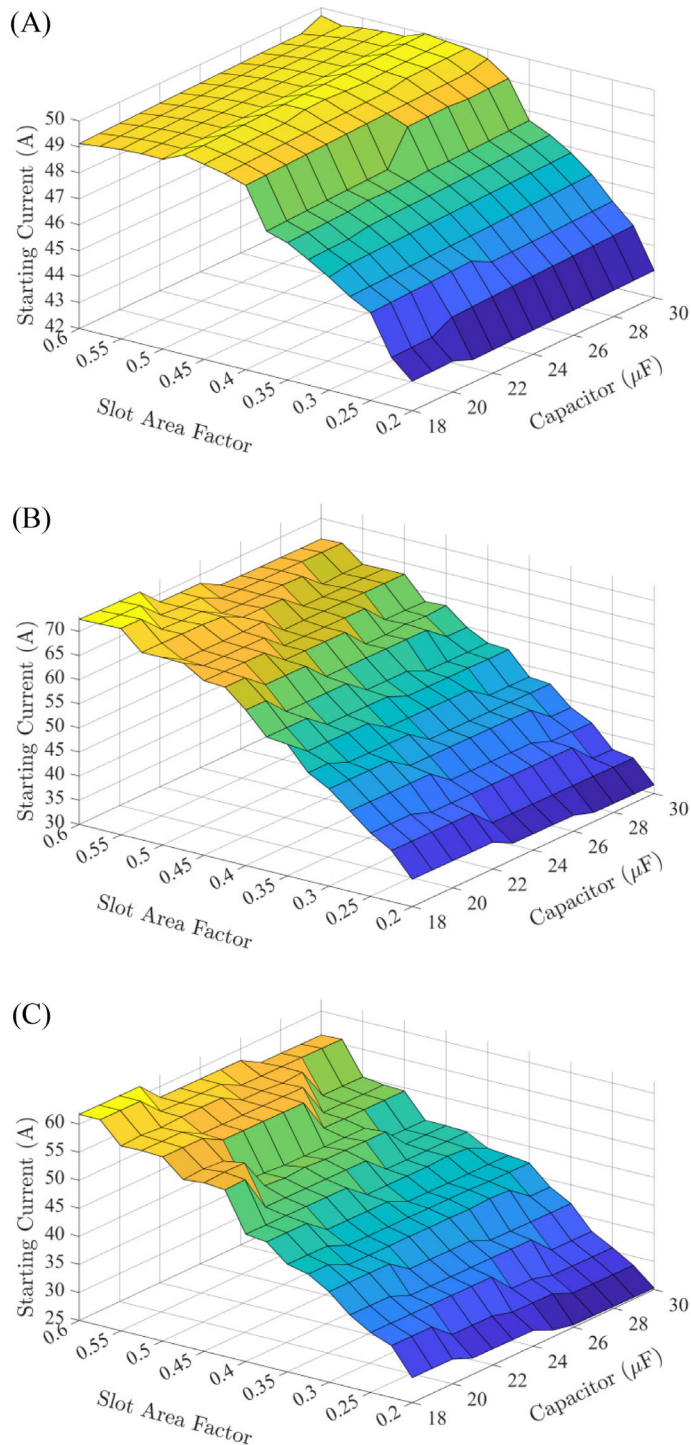
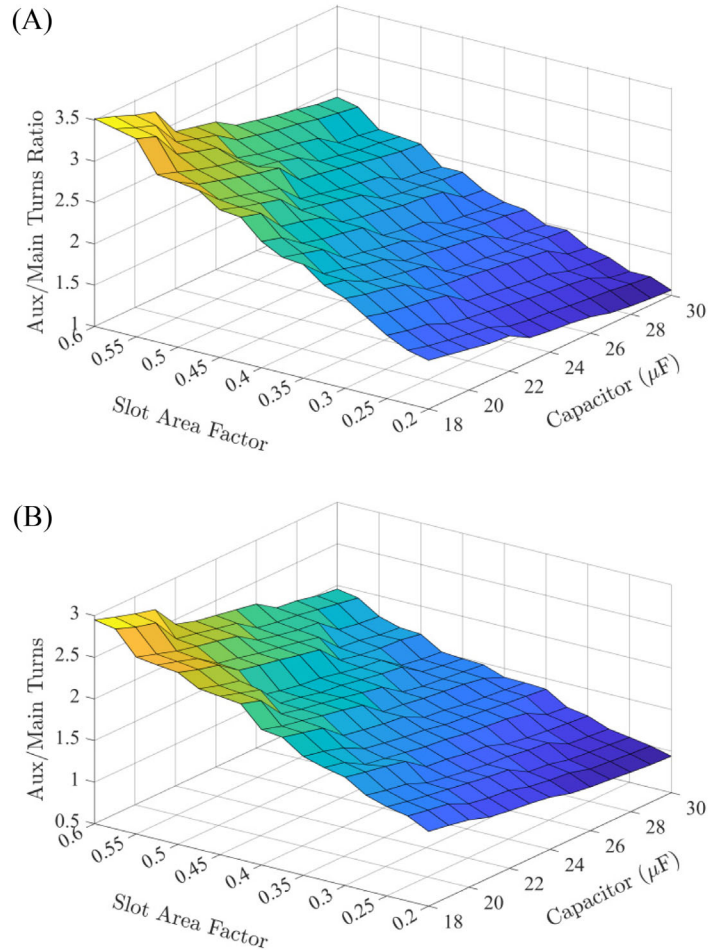


FIGURE 8 Variation of SPIM starting current as a function of C_{run} and k_{bar} for (A) “Method-A,” (B) “Method-B,” and (C) Method-C

FIGURE 9 Variation of auxiliary to main windings turns ratio (a) as a function of C_{run} and k_{bar} for (A) “Method-B” and (B) “Method-C.” It is to be noted that for “Method-A” the parameter a is kept constant and thus no variation applies



starting current ranges from 42 to 49 A. Thus, the SPIM topologies derived from Method-A failed to meet the set constraint regarding the starting to nominal current ratio (I_{st}/I_n) given in Table A1 in the Appendix. For Method-B and Method-C a detailed comparison is presented in Table 1, where the minimum and the maximum recorded starting current are given along with the k_{bar} variation range. The minimum and the maximum starting current were obtained for $C_{\text{run}} = 30$ and 18 μF respectively. Based on the data provided there, the SPIM configurations derived from Method-B exhibit 16% up to 33% higher starting current than the corresponding ones obtained from Method-C. Thus, it can be easily said that the motor's axial effective length increment (a crucial modification according to the author's proposals) benefits significantly the starting performance.

3.5 | Auxiliary to main windings turns ratio

As the rotor bar slot cross-sectional area becomes larger, a higher value has to be assigned to the parameter a , aiming the motor to satisfy the set requirements regarding the T_{st}/T_n ratio. This results to a larger number for the auxiliary winding turns number (N_a), which increases extensively the stator copper losses and therefore reduces the motor's efficiency. For k_{bar} equal or lower than 0.375, the turns ratio variation range seems to comply with the relative directions provided in Reference 32 for the majority of the examined SPIM models. However, when k_{bar} is set equal to 0.2 the turns ratio value ranges from 0.9 to 1.5. A value lower than 1.0 has to be adopted when a capacitor of high value is used. Generally, as the capacitance increases, the turns ratio value decreases. The efficiency is maximized for a turns ratio value equal to 1.0. Thus, it can be said that: (a) the turns ratio has great effect both on SPIM nominal and starting performance, (b) its value has to be set under investigation and is strongly related with the capacitor value and (c) the examined variation range which leads to SPIM with premium-efficiency is quite different from the one proposed in Reference 32.

Comparing the motor topologies derived from Method-B and Method-C (Figure 9), it can be said that that a higher turns ratio is always required when Method-B is applied. This leads to motor topologies with larger copper windings mass

k_{bar} value	min. I_{st} (A)		max. I_{st} (A)	
	Method-B	Method-C	Method-B	Method-C
0.200	31.78	25.28	35.68	29.46
0.225	37.71	28.69	41.46	34.27
0.250	38.50	30.62	44.02	35.67
0.275	42.97	32.61	47.52	37.90
0.300	45.09	36.67	51.05	41.13
0.325	48.91	38.69	53.33	43.35
0.350	49.33	42.51	58.13	44.97
0.375	53.91	42.86	58.62	47.26
0.400	54.23	43.37	63.19	47.72
0.425	56.41	44.83	66.87	54.85
0.450	59.63	45.06	67.13	54.93
0.475	59.87	45.09	69.74	55.28
0.500	64.35	49.39	69.85	57.85
0.525	64.36	49.59	69.94	58.06
0.550	64.45	51.46	73.54	59.19
0.575	67.62	55.73	73.61	61.73
0.600	67.47	55.89	73.75	61.77

TABLE 1 Minimum and maximum starting current (I_{st}) for the SPIM topologies derived from “Method-B” and “Method-C”

and consequently a higher manufacturing cost. On the contrary, Method-C seems to present another important advantage in this matter.

4 | COMPARISON OF THE RESULTED TOPOLOGIES AND DISCUSSION

In this section, a comprehensive comparison of the SPIM topologies derived from the three examined design methods is made. As already mentioned the SPIM configurations obtained from Method-A failed to satisfy the efficiency requirements according to the data provided in Table A2 in the Appendix. Thus, the specific design method is not investigated and commented further. The performance characteristics of the SPIMs which presented the highest efficiency (achieved when k_{bar} is equal to 0.2) are summarized in Tables A3 and A4 in the Appendix. Regarding Method-B and Method-C, the following are observed:

1. Method-C results to topologies with higher efficiency for the whole variation range of k_{bar} , as it can be seen in Table 2. In this table, the achieved efficiency ratings are characterized according to the efficiency classes defined by the latest

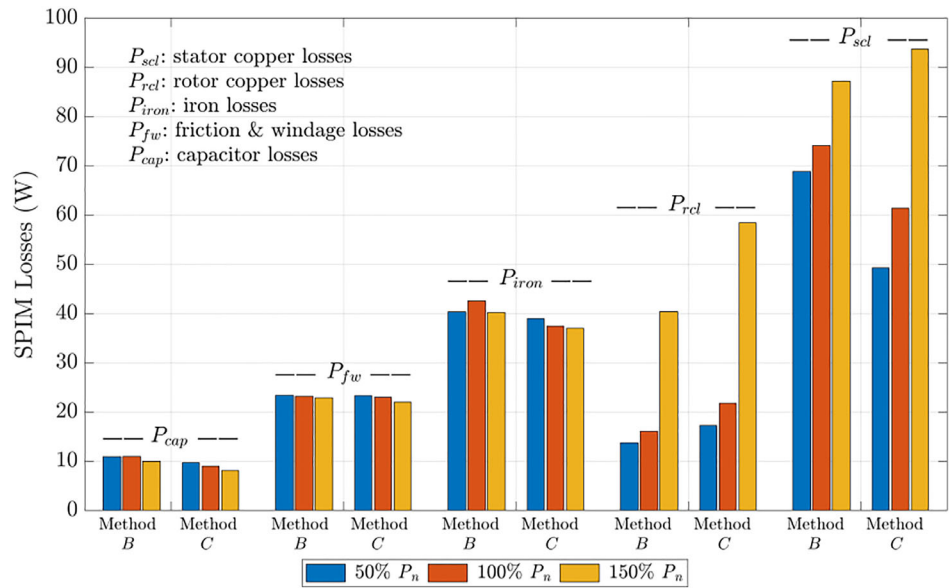
k_{bar}	Method-B	Method-C
0.200	IE2-IE3/IE3-IE4	IE3-IE4
0.225	IE2-IE3	IE2-IE3/IE3-IE4
0.250	IE1-IE2/IE2-IE3	IE2-IE3/IE3
0.275	IE1-IE2/IE2-IE3	IE2-IE3
0.300	IE1-IE2	IE1-IE3
0.325	IE1-IE2	IE1-IE2
0.350	IE1-IE2	IE1-IE2
0.375	IE1-IE2	IE1-IE2
0.400	IE0	IE1-IE2
0.425	IE0	IE1-IE2
0.45-0.6	IE0	IE0

TABLE 2 Efficiency ratings comparison for the SPIMs derived from “Method-B” and “Method-C” for different k_{bar} values

TABLE 3 Efficiency and power factor comparison for the SPIM topologies (with $C_{\text{run}} = 18 \text{ uF}$ and $k_{\text{bar}} = 0.2$) for different load conditions

SPIM loading (% P_{out})	Method-A		Method-B		Method-C	
	η (%)	$\cos \phi$	η (%)	$\cos \phi$	η (%)	$\cos \phi$
25%	45.38	0.317	53.52	0.484	55.26	0.641
50%	62.75	0.438	70.34	0.671	72.91	0.833
75%	72.01	0.554	77.78	0.802	80.14	0.919
100%	78.19	0.676	81.72	0.885	83.02	0.951
125%	80.47	0.744	84.25	0.944	83.92	0.969
150%	82.36	0.816	84.80	0.959	83.61	0.979

FIGURE 10 Comparison regarding the particular losses of the topologies (with $C_{\text{run}} = 18 \text{ uF}$ and $k_{\text{bar}} = 0.2$) derived from “Method-B” and “Method-C” for three loading conditions



international standards. For 4-poles 1.0 HP SPIM, the minimum efficiency values are equal to: 72.1%, 79.6%, 82.5%, and 85.7% for IE1 (standard efficiency), IE2 (high efficiency), IE3, and IE4 respectively. When the motor exhibits efficiency lower than 72.1%, its efficiency rating is characterized as IE0 (ie, below efficiency standards).

- Method-B results to efficiencies which vary between IE3 and IE4 when $k_{\text{bar}} = 0.2$ and C_{run} is equal or higher than 23 uF. On the other hand, an efficiency of the same ratings can be achieved for Method-C when k_{bar} is equal to both 0.2 and 0.225. In these cases, the desirable efficiency can be reached even for low values of C_{run} .
- From Tables A3 and A4 in the Appendix, it can be seen that the efficiency at nominal operation of the SPIMs obtained from Method-C is higher by 0.37% up to 2.03% than those of the topologies derived from Method-B.
- The performance of the SPIMs obtained from Method-C is also superior for the majority of the examined motor's operational conditions, as it can be concluded from Table 3, where the relevant results are given for $C_{\text{run}} = 18 \text{ uF}$. Method-C contributes to important energy savings resulting to both higher efficiency and power factor when the motor operates at nominal and sub-nominal conditions. The topologies derived from Method-B exhibit slightly higher efficiency when the SPIM operates under overload conditions. Further information regarding the particular losses (stator windings copper (P_{scf}), rotor copper (P_{rcf}), iron (P_{iron}), capacitor (P_{cap}), and friction & windage (P_{fw}) losses) of the obtained SPIM topologies (with $C_{\text{run}} = 18 \text{ uF}$) for three different operating points is provided in Figure 10.
- When Method-B is adopted, a higher number of turns for the main and the auxiliary winding is used. Thus, the copper mass and consequently the motor's net total mass is also larger. The masses of the SPIM topologies of Method-B are larger than the corresponding ones of Method-C by 0.82 kg up to 1.12 kg. Furthermore, their manufacturing cost is also increased. The authors calculated the cost of the SPIMs taking into account: (a) the mass of the different motor's parts and (b) the materials' price retrieved through the conduction of thorough search in the international materials market (the cost of the used run-capacitor is excluded). The obtained results are given in Tables A3 and A4 in the Appendix. It can be seen that the cost of the SPIMs of Method-B is higher by 12.4% up to 15.63%.

6. When the Method-B is followed, the SPIMs present higher core losses by 13.3% up to 19.5%. The core losses density varies from 4.7 to 5.1 W/kg for these configurations. For the topologies of Method-C the specific quantity ranges from 4 to 4.5 W/kg. The increment of the motor's axial effective length contributes to the core losses reduction. No magnetic saturation has been observed at the examined SPIM models.
7. Method-C results to SPIMs with lower starting to nominal current ratio (I_{st}/I_n), as already demonstrated in Section 3. This ratio varies from 6.5 up to 7.17 for the case of Method-C. In the case of Method-B, the specific ratio is almost equal to 8.

5 | PROPOSED SPIM DESIGN METHODOLOGY

5.1 | Description

In this section, an overall integrated design methodology is proposed for the development of capacitor-run SPIMs that exhibit both: (a) satisfactory starting performance and (b) efficiency at least equal or even higher than that defined by IE3 efficiency class. The methodology (depicted in flowchart form in Figure 11) is based on the conclusions extracted through the post-processing analysis and comparison of the so far obtained results (presented in Sections 3 and 4). A description of the most important steps and features follows.

The design procedure starts with the specification of: (a) the SPIM's characteristics (eg, output power, efficiency, power factor, starting torque, and so on) and (b) the imposed constraints (eg, maximum acceptable values for starting current and main/auxiliary windings current density, and so on). Next, the methodology incorporates the steps (described in Section 2.2) that were adopted in Method-C for the calculation of the motor's basic dimensions (ie, D_o , D , and L). It is reminded that Method-C presents clear advantages compared to the other two examined methods taking into consideration several motor's performance characteristics and various indexes.

The process continues with the selection of stator/rotor slots (Q_s/Q_r) combination. This feature affects substantially both the SPIM's efficiency (as already highlighted in Reference 31) and overall performance. When the proper combination is chosen, various parasitic and undesirable phenomena (eg, asynchronous harmonic torques, synchronous torques during motor's running due to the extensive harmonic slots, mechanical vibrations, noisy operation, and so on) can be reduced or even eliminated. Reader can refer to Reference 33 aiming to find further information about the combinations that contribute to this direction.

Regarding the rotor bar slot design, the authors suggest the k_{bar} to be set equal to 0.2. It has been proven that a rotor bar slot with small cross-sectional area benefits both the SPIM's starting torque and efficiency at running condition. Furthermore, it has been demonstrated that the variation range for k_{bar} proposed in Reference 32, does not contribute to the SPIMs efficiency improvement toward IE3. Afterwards, the stator, rotor, and end-ring geometrical parameters are calculated as described in Section 2.1.

Then, N_m , a , and C_{run} are determined. The design methodology is based on loops, taking into account the impact of the above design parameters on the capacitor-run SPIM's performance. Specifically, high priority has been given to the parameters whose effect on efficiency is greater. Based on the obtained results, it is clear that the desirable efficiency ratings as well as satisfactory starting torque are achievable when N_m and a are properly selected. This is feasible even when a low value is used for C_{run} . Regarding parameter a , it is recommended to range from 1.5 down-to 0.8. The value of C_{run} is re-calculated when a different value is assigned to a .

For given N_m and N_a , the wire diameters of the main and auxiliary winding are calculated taking into account the stator slot area (A_s) and the considered slot fill factor (sf). The slot fill factor is specified taking into account the wire type, the stator slot shape and the winding assembly technique that is going to be used. Aiming to guarantee the SPIM's overall high performance, the main/aux. windings current density (J_m , J_a) are also included among the set requirements. The maximum acceptable value for these parameters is suggested to be set equal to 3.5 A/mm².

Consequently, the presented methodology: (a) diminishes the number of the important design parameters that have to be set under investigation, (b) limits their search space (ie, taking into account the directions provided for C_{run} and a), and (c) reduces the problem's complexity and computational time. Following this methodology, SPIMs designers and manufacturers would be able to create an initial SPIM topology (through not optimized), performing only a small number of FEA simulations. This initial design will satisfy all the set requirements and be in accordance with the latest international industrial standards.

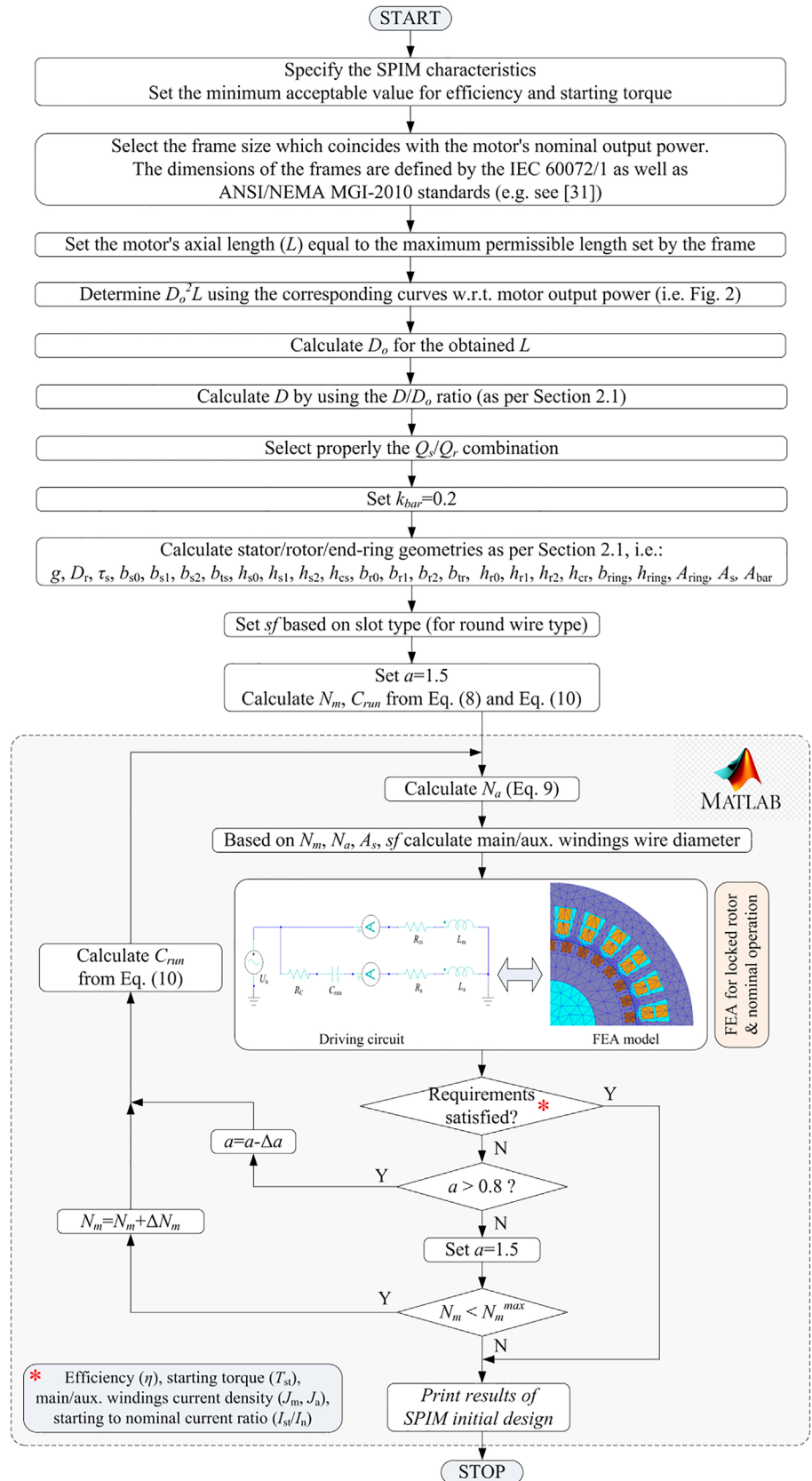


FIGURE 11 Flowchart of the proposed capacitor-run SPIMs design methodology

SPIM under study	η (%)	$\cos \phi$	n_m (rpm)	C_{run} (μ F)	a	N_a	N_m	I_{st}/I_n
0.25 HP	74.48	0.912	1440	4.5	1.500	1182	788	4.98
0.50 HP	80.32	0.937	1455	9.0	1.455	768	528	6.69

TABLE 4 Performance characteristics and design parameters of the obtained SPIM topologies with horsepower equal to 0.25 HP and 0.50 HP

5.2 | Further validation and results

In this section, the proposed design methodology is applied to capacitor-run SPIMs with different output power ratings (0.25 and 0.5 HP) and specifications aiming to further validate its effectiveness. The relevant SPIMs operational characteristics and constraints are summarized in the last two columns of Table A1 in the Appendix. The minimum efficiency that the motors have to present is in accordance with the latest efficiency standards, while the rest specifications have been retrieved from the commercial catalogs of SPIMs manufacturers. The motors have 24 stator slots and a copper rotor squirrel-cage with 30 bars. Moreover, the stator and rotor slot configurations depicted in Figure 1 have been used.

Utilizing the proposed design methodology, we obtain the following:

(a) frame size: “63,” $D_o = 100$ mm, $D = 61.23$ mm, and $L = 80$ mm for the 0.25 HP SPIM.

(b) frame size: “80,” $D_o = 121.44$ mm, $D = 73.47$ mm, and $L = 100$ mm for the 0.50 HP SPIM.

The derived SPIM topologies satisfy all the set requirements, as it can be seen from the data provided in Table 4. The achieved efficiency ratings are higher than those defined by IE3 efficiency class (given in Table A1 in the Appendix) and they are very close to the corresponding ones imposed by IE4. According to IE4, the minimum acceptable efficiency is equal to 74.7% and 81.1% for a 0.25 HP and 0.50 HP 4-poles SPIM respectively. Thus, it is obvious that the proposed design methodology is applicable to a wide variety of capacitor-run SPIMs with different output power ratings and can contribute to significant efficiency improvement and energy savings.

Furthermore, the SPIM desirable performance is achievable even for a low value of C_{run} . It is noted that the value of the run-capacitor used in 0.25 HP commercial SPIMs ranges from 4.5 to 10 μ F. The same parameter ranges from 9 to 18 μ F in the case of 0.50 HP commercial SPIMs. In any case, following this design methodology an initial SPIM design can be derived which comply with the latest international industrial standards and could be the starting point for further optimization-focused research studies.

6 | CONCLUSIONS

This work presented a cost-effective design methodology for the development of capacitor-run SPIMs with satisfactory starting performance and enhanced efficiency in accordance with the latest international industrial standards. In the proposed design process the motor frame sizes as well as several operating constraints have been taken into account. Additionally, the effectiveness of the design methodology has been validated through its application to motors with different output power ratings and specifications. It has been proven that it can contribute to significant energy savings and SPIMs topologies that are advantageous from manufacturing and economical point of view. Moreover, the authors highlighted the impact of crucial design parameters (ie, rotor bar cross-sectional area, capacitor value, auxiliary to main windings turns ratio) on the motor's performance. Some of them have not been adequately investigated in the available literature. Thus, many useful conclusions have been extracted and a large number of directions are provided in this work. These directions are quite different from the corresponding ones found in the classical SPIM design literature and could be of great help to engineers, designers and manufacturers.

PEER REVIEW INFORMATION

Engineering Reports thanks Huai-Cong Liu, Damir Žarko, and other anonymous reviewer(s) for their contribution to the peer review of this work.

CONFLICT OF INTEREST

The authors declare no potential conflict of interest.

ORCID

Yannis L. Karnavas  <https://orcid.org/0000-0002-7390-3249>

REFERENCES

1. Sarac V, Trajchevski N. Impact of capacitor on operating characteristics of single-phase motor. Paper presented at: Proceedings of 2019 16th Conference on Electrical Machines, Drives and Power Systems (ELMA); June 6–8, 2019; Varna, Bulgaria. <https://doi.org/10.1109/ELMA.2019.8771599>.
2. Rasmussen CB, Miller TJE. Revolving-field polygon technique for performance prediction of single-phase induction motors. *IEEE Trans Indus Appl*. 2003;39(5):1300–1306. <https://doi.org/10.1109/TIA.2003.816563>.
3. Ferreira FJTE, Ge Baoming AT d A. Reliability and operation of high-efficiency induction motors. *IEEE Trans Indus Appl*. 2016;52(6):4628–4637. <https://doi.org/10.1109/TIA.2016.2600677>.
4. Sarac V, Atanasova-Pacemka T. Multi parameter analysis for efficiency improvement of single-phase capacitor motor. *Math Probl Eng*. 2019;2019:5131696. <https://doi.org/10.1155/2019/5131696>.
5. Lubin T, Mezani S, Rezzoug A. Analytic calculation of eddy currents in the slots of electrical machines: application to cage rotor induction motors. *IEEE Trans Magnet*. 2011;47(11):4650–4659. <https://doi.org/10.1109/TMAG.2011.2157167>.
6. Sen Kurt M, Fenercioglu A. Rotor slot distance effects on output parameters in single phase induction motors. *Hittite J Sci Eng*. 2018;5(1):31–35. <https://doi.org/10.17350/HJSE19030000075>.
7. Lee HJ, Im SH, Um DY, Park GS. A design of rotor bar for improving starting torque by analyzing rotor bar resistance and reactance in squirrel cage induction motor. *IEEE Trans Magnet*. 2018;54(3):1–4. <https://doi.org/10.1109/TMAG.2017.2764525>.
8. Zhou GY, Shen JX. Current harmonics in induction machine with closed-slot rotor. *IEEE Trans Indus Appl*. 2017;53(1):134–142. <https://doi.org/10.1109/TIA.2016.2609851>.
9. Zhang D, Park CS, Koh CS. A new optimal design of rotor slot of three-phase squirrel cage induction motor for NEMA class D speed-torque characteristic using multi-objective optimization algorithm. *IEEE Trans Magnet*. 2012;48(2):879–882. <https://doi.org/10.1109/TMAG.2011.2174040>.
10. Mach M, Cipin R, Toman M, Hajek V. Impact of number of rotor slots on performance of three-phase and single-phase induction machines. Paper presented at: Proceedings of 2018 IEEE International Conference on Environment and Electrical Engineering and 2018 IEEE Industrial and Commercial Power Systems Europe (EEEIC/I&CPS Europe); June 12–15, 2018; Palermo, Italy. <https://doi.org/10.1109/EEEIC.2018.8494514>.
11. Andersen PS, Dorrell DG, Weihrauch NC, Hansen PE. Synchronous torques in split-phase induction motors. *IEEE Trans Indus Appl*. 2010;46(1):222–231. <https://doi.org/10.1109/TIA.2009.2036199>.
12. Heo CG, Kim HM. A design of rotor bar inclination in squirrel cage induction motor. *IEEE Trans Magnet*. 2017;53(11):1–4. <https://doi.org/10.1109/TMAG.2017.2696977>.
13. Finley WR, Hodowanec MM. Selection of copper versus aluminum rotors for induction motors. *IEEE Trans Indus Appl*. 2001;37(6):1563–1573. <https://doi.org/10.1109/28.968162>.
14. da Silva CA, Gibelli GB, Pereira JF, Alvey A, Carlson R. Analysis of single-phase induction motors with centrifuged rotors. Paper presented at: Proceedings of 2013 International Electric Machines & Drives Conference (IEMDC); May 12–15, 2013; Chicago, IL, USA:1305–1309. <https://doi.org/10.1109/IEMDC.2013.6556327>.
15. Lee KS, Ho Lee S, Park JH, Kim JM, Choi JY. Experimental and analytical study of single-phase squirrel-cage induction motor considering end-ring porosity rate. *IEEE Trans Magnet*. 2017;53(11):1–4. <https://doi.org/10.1109/TMAG.2017.2714190>.
16. Liu Y, Han P, Bazzi AM. A comparison of rotor bar material of squirrel-cage induction machines for efficiency enhancement purposes. Paper presented at: Proceedings of 2015 17th European Conference on Power Electronics and Applications (EPE'15 ECCE-Europe); Sept. 8–10, 2015; Geneva, Switzerland. <https://doi.org/10.1109/EPE.2015.7311778>.
17. Chasiotis ID, Karnavas YL. Investigation on single phase induction motor efficiency and starting capability enhancement by incorporating magnesium alloys rotors. *Int Sci J Mach Technol Mater*. 2020;1:16–19.
18. Ling Z, Zhou L, Li H, Zhu W, Guo S, Wang J. The use of electrical steels in single-phase induction machines and the modified iron loss test method. *IEEE Trans Magnet*. 2014;50(11):1–4. <https://doi.org/10.1109/TMAG.2014.2329031>.
19. Mallard V, Parent G, Demian C, Brudny JF, Delamotte A. Increasing the energy efficiency of induction machines by the use of grain-oriented magnetic materials and die casting copper squirrel cage in the rotor. *IEEE Trans Indus Appl*. 2019;55(2):1280–1289. <https://doi.org/10.1109/TIA.2018.2873532>.
20. Wang S, Kang J, Noh J. Topology optimization of a single-phase induction motor for rotary compressor. *IEEE Trans Magnet*. 2004;40(3):1591–1596. <https://doi.org/10.1109/TMAG.2004.827187>.
21. Szabo L. A survey on the efficiency improve of electrical machines. Paper presented at: Proceedings of 2019 26th International Workshop on Electric Drives; Improvement in Efficiency of Electric Drives (IWED); Jan. 30–Feb. 02, 2019; Moscow, Russia. <https://doi.org/10.1109/IWED.2019.8664220>.
22. Iorgulescu M. Study of single phase induction motor with aluminium versus copper stator winding. Paper presented at: Proceedings of 2016 International Conference on Applied and Theoretical Electricity (ICATE); Oct. 6–8, 2016; Craiova, Romania. <https://doi.org/10.1109/ICATE.2016.7754643>.
23. Mera R, Campeanu R. Optimal performance of capacitor-run single phase induction motor. Paper presented at: Proceedings of 2012 13th International Conference on Optimization of Electrical and Electronic Equipment (OPTIM); May 24–26, 2012; Brasov, Romania. <https://doi.org/10.1109/OPTIM.2012.6231966>.

24. Hosseini SM. Performance improvement of capacitor-run single-phase induction motor by non-orthogonal armature windings. Paper presented at: Proceedings of 2016 International Symposium on Power Electronics, Electrical Drives, Automation and Motion (SPEEDAM); June 22–24; Anacapri, Italy:1336–2016. <https://doi.org/10.1109/SPEEDAM.2016.7525872>.
25. Debusschere V, Multon B, Ben Ahmed H, Cavarec PE. Life cycle design of a single-phase induction motor. *IET Electr Power Appl*. 2010;4(5):348–356. <https://doi.org/10.1049/iet-epa.2009.0173>.
26. Yousefian M, Mosaddegh HR, Zarchi HA. Optimal design of a single-phase two-value capacitor induction motor with fan load. Paper presented at: Proceedings of Iranian Conference on Electrical Engineering (ICEE); May 8–10, 2018; Mashhad, Iran. <https://doi.org/10.1109/ICEE.2018.8472466>.
27. Subramanian S, Bhuvaneswari R. Optimal design of single-phase induction motor using particle swarm optimization. *Int J Comput Math Electr Electron Eng*. 2007;26(2):418–430. <https://doi.org/10.1108/03321640710727773>.
28. Wang X, Zhong H, Yang Y, Mu X. Study of a novel energy efficient single-phase induction motor with three series-connected windings and two capacitors. *IEEE Trans Energy Convers*. 2010;25(2):433–440. <https://doi.org/10.1109/TEC.2009.2039218>.
29. Mohammed KG, Ramli AQ. Analyzing the performance of completed designed outer rotor single phase induction motor. Paper presented at: Proceedings of 2013 IEEE Student Conference on Research and Development (SCoReD); Dec. 16–17, 2013; Putrajaya, Malaysia. <https://doi.org/10.1109/SCoReD.2013.7002579>.
30. Dorrell DG. A review of the methods for improving the efficiency of drive motors to meet IE4 efficiency standards. *J Power Electron*. 2014;14(5):842–851. <https://doi.org/10.6113/JPE.2014.14.5.842>.
31. Karnavas YL, Chasiotis ID. Design and manufacturing of a single-phase induction motor: a decision aid tool approach. *Int Trans Electr Energy Syst*. 2017;27(9):e2357. <https://doi.org/10.1002/etep.2357>.
32. Boldea I, Nasar SA. *The Induction Machines Design Handbook*. 2nd ed. Boca Raton, FL: CRC Press; 2010 845 pages, ISBN: 9781420066685—CAT# 66684.
33. Pyrhonen J, Jokinen T, Hrabovcova V. *Design of Rotating Electrical Machines*. 2nd ed. West Sussex, UK: John Wiley & Sons Ltd, ISBN: 978-1-118-58157-5; 2013.
34. Um DY, Park GS. Determination scheme of stator parameters for making rotating fields circular in a single-phase induction motor. *IEEE Trans Magnet*. 2020;56(1):1–5. <https://doi.org/10.1109/TMAG.2019.2949031>.
35. Premium efficiency motor selection and application guide – A handbook for industry. U.S. Dept. of Energy, Energy Efficiency & Renewable Energy, Advanced Manufacturing Office. [Online]. https://www.energy.gov/sites/prod/files/2014/04/f15/amo_motors_handbook_web.pdf. Accessed June 18, 2020.

How to cite this article: Chasiotis ID, Karnavas YL. A novel design methodology for the compliance of single phase induction motors with recent industrial premium efficiency standards. *Engineering Reports*. 2020;e12265. <https://doi.org/10.1002/eng2.12265>

APPENDIX A

Parameter	1.0 HP	0.5 HP	0.25 HP
Output power (rated), P_n	746 W	373 W	186.5 W
Output torque (rated), T_n	≥ 4.8 Nm	≥ 2.5 Nm	≥ 1.2 Nm
Speed (rated), n_m	≥ 1420 rpm	≥ 1420 rpm	≥ 1420 rpm
Line current (rated), I_n	≤ 5.0 A	≤ 2.5 A	≤ 1.5 A
Power factor, $\cos \phi$	≥ 0.9	≥ 0.9	≥ 0.9
Efficiency (at 100% load), η	$\geq 82.5\%$	$\geq 77.3\%$	$\geq 69.9\%$
Starting to nominal torque ratio, T_{st}/T_n	≥ 0.35	≥ 0.40	≥ 0.50
Starting to nominal current ratio, I_{st}/I_n	≤ 8.0	≤ 7.5	≤ 5.0
Supply voltage, U_n	230 V	230 V	230 V
Supply frequency, f	50 Hz	50 Hz	50 Hz
Number of poles, $2p$	4	4	4
Net mass, M	≤ 14.0 kg	≤ 8.0 kg	≤ 5.0 kg

TABLE A1 SPIMs desirable operational characteristics and relevant constraints

TABLE A2 Performance characteristics of the SPIM topologies obtained from “Method-A” for $k_{\text{bar}} = 0.2$

$C_{\text{run}} (\mu\text{F})$	$\eta (\%)$	$\cos \phi$	T_{st}/T_n	$I_{st} (\text{A})$
18	78.19	0.676	0.350	43.14
19	78.21	0.682	0.370	43.16
20	78.16	0.688	0.394	43.19
21	76.89	0.694	0.414	42.88
22	76.77	0.701	0.439	42.89
23	76.63	0.707	0.464	42.91
24	76.44	0.719	0.488	42.93
25	76.17	0.732	0.515	42.95
26	75.89	0.745	0.540	42.96
27	75.56	0.759	0.566	42.99
28	75.18	0.772	0.593	43.00
29	74.76	0.786	0.619	43.03
30	74.31	0.800	0.646	43.04

TABLE A3 Performance characteristics and design parameters of the SPIM topologies obtained from “Method-B” for $k_{\text{bar}} = 0.2$

$C_{\text{run}} (\mu\text{F})$	$\eta (\%)$	$\cos \phi$	a	N_a	N_m	$I_{st} (\text{A})$	I_{st}/I_n	$M (\text{kg})$	Cost (\$)
18	81.72	0.885	1.592	624	392	35.677	7.96	13.13	49.32
19	81.97	0.889	1.541	604	392	35.637	8.01	13.21	49.76
20	81.83	0.894	1.500	588	392	35.595	8.02	13.07	48.97
21	81.69	0.897	1.449	568	392	35.546	8.03	12.99	48.53
22	81.50	0.906	1.429	560	392	35.544	8.09	12.96	48.35
23	83.06	0.944	1.290	516	400	33.391	8.06	12.78	47.28
24	82.94	0.948	1.260	504	400	33.346	8.07	12.76	47.17
25	82.78	0.954	1.240	496	400	33.322	8.12	12.70	46.86
26	82.70	0.957	1.200	480	400	33.263	8.09	12.64	46.51
27	83.52	0.976	1.127	460	408	31.918	8.02	12.57	46.13
28	83.43	0.977	1.098	448	408	31.862	7.99	12.53	45.88
29	83.30	0.981	1.078	440	408	31.821	8.02	12.50	45.71
30	83.16	0.984	1.059	432	408	31.787	8.04	12.47	45.54

TABLE A4 Performance characteristics and design parameters of the SPIM topologies obtained from “Method-C” for $k_{\text{bar}} = 0.2$

$C_{\text{run}} (\mu\text{F})$	$\eta (\%)$	$\cos \phi$	a	N_a	N_m	$I_{st} (\text{A})$	I_{st}/I_n	$M (\text{kg})$	Cost (\$)
18	83.02	0.951	1.400	504	360	29.460	7.17	12.14	43.35
19	82.94	0.956	1.356	488	360	29.427	7.18	12.08	43.03
20	82.82	0.958	1.311	472	360	29.387	7.18	12.03	42.72
21	83.31	0.978	1.228	452	368	27.914	7.01	11.94	42.24
22	83.53	0.980	1.196	440	368	27.870	7.03	11.80	42.01
23	83.43	0.983	1.163	428	368	27.838	7.04	11.86	41.78
24	83.35	0.985	1.130	416	368	27.796	7.03	11.82	41.55
25	83.68	0.995	1.053	400	380	26.181	6.73	11.78	41.29
26	84.09	0.999	1.021	392	384	25.424	6.58	11.74	41.11
27	84.01	0.999	1.000	384	384	25.387	6.56	11.72	40.96
28	83.93	1.000	0.969	372	384	25.346	6.55	11.68	40.77
29	83.84	1.000	0.948	364	384	25.307	6.54	11.65	40.59
30	83.76	1.000	0.938	360	384	25.276	6.52	11.64	40.52